BMC Medical Imaging

RESEARCH

Open Access

Development and validation of a CT-based radiomics nomogram for predicting progression-free survival in patients with small cell lung cancer

Nan Yang[1,3†], Zhuang Xuan Ma[1,3†], Xin Wang[2], Li Xiao[2], Liang Jin[1,3*] and Ming Li[1,3*]

Abstract

Purpose Small cell lung cancer (SCLC) is a highly aggressive form of lung cancer, representing about 15% of cases worldwide. Despite advances in imaging, such as low-dose CT, which have increased diagnostic rates, survival outcomes for SCLC patients have remained stagnant. Recent studies have only focused on radiomics, which extracts detailed quantitative features from imaging, with clinical risk factors to improve prognostic models. Therefore, this study aimed to develop a clinical-radiomics fusion nomogram based on computed tomography (CT) to estimate progression-free survival (PFS) in patients diagnosed with SCLC. By integrating radiomics features extracted from CT with clinical data, this model provides personalized prognostic assessment for clinicians. Its clinical utility lies in aiding treatment decision-making by offering more accurate prognostic evaluation, optimizing therapeutic strategies, and identifying high-risk patients at an early stage, ultimately improving overall survival and quality of life.

Methods To develop the nomogram model, 95 patients diagnosed with pathologically confirmed SCLC between January 1, 2013, and December 31, 2023, were included in the study cohort. Participants were randomly divided into training and validation cohorts in a 7:3 ratio. Radiomics features associated with PFS were generated using the least absolute shrinkage and selection operator (LASSO) along with univariate and multivariate analyses. Additionally, in the training cohort, both univariate and multivariate analyses using Cox regression were conducted to identify the significant clinical risk factors influencing PFS. The predictive performance of the clinical and clinical-radiomics fusion nomogram were evaluated using the concordance index, calibration plots, and decision curve analysis (DCA).

Results Five radiomics features were selected and used to calculate the radiomics score (Rad-score). The radiomics features were significantly associated with PFS (hazard ratio: 0.5765, 95% confidence interval: 0.3641–0.9128, $p < 0.05$). Three clinical risk factors significantly associated with PFS were identified: neuron-specific enolase (NSE), carbohydrate antigen 125 levels (CA125), and treatment type, such as surgery. The clinical-radiomics fusion nomogram model

†Nan Yang and Zhuang Xuan Ma contributed equally to this work.

*Correspondence:
Liang Jin
jin_liang@fudan.edu.cn
Ming Li
ming_li@fudan.edu.cn

Full list of author information is available at the end of the article

(C-index:0.744) demonstrated superior performance compared to the clinical nomogram model (C-index: 0.718) in the training cohort. DCA indicated that the clinical-radiomics fusion nomogram outperformed the clinical nomogram in terms of clinical usefulness.

Conclusions A CT-based clinical-radiomics fusion nomogram was developed to predict PFS in patients with SCLC, which is useful in providing individualized information.

Advances in knowledge A clinical-radiomics fusion nomogram was constructed to estimate the probability of PFS based on clinical risk factors and the rad-score.

Keywords Radiomics, Nomogram, Small-cell lung cancer, Progression-free survival, Computed tomography

Introduction

Lung cancer, which remains the leading cause of cancer-related mortality globally and has the highest incidence among malignant tumors [1, 2]. SCLC is a high-grade neuroendocrine cancer characterized by low differentiation, rapid proliferation, and early metastasis. Despite SCLC accounting for approximately 15% of lung cancer cases in countries such as the USA, UK, China, and Korea, the precise global burden of SCLC remains difficult to estimate due to geographical and ethnic variations [3]. Currently, SCLC is categorized into limited-stage(LS-SCLC) and extensive-stage(ES-SCLC) based on widely used staging criteria [4]. Alarmingly, about 70% o patients are diagnosed with ES-SCLC at initial presentation, which is associated with a poor prognosis [5].

Advancements in imaging techniques, particularly thin-slice CT, have improved the detection rate of SCLC [1]. However, despite the increased diagnostic accuracy, survival outcomes for SCLC patients have remained stagnant [6]. The standard treatment approach for LS-SCLC involves chemotherapy, along with concurrent or sequential thoracic or mediastinal radiotherapy [7]. Although SCLC is highly responsive to chemotherapy and radiotherapy, relapse occurs in a significant proportion of patients within six months of treatment [8]. Platinum-based chemotherapy, specifically the combination of platinum and etoposide, is widely accepted as the standard treatment for both LS-SCLC and ES-SCLC [9, 10]. The role of surgical resection in SCLC remains controversial, with only a minority of patients being considered suitable candidates [11]. More recently, immunotherapy has emerged as a promising therapeutic option, particularly through the use of immune checkpoint inhibitors in combination with chemotherapy, which is now the standard first-line treatment for ES-SCLC [12]. Despite these advances, the overall prognosis for SCLC remains poor, with a five-year survival rate of only 20–25% for LS-SCLC and as low as 2% for ES-SCLC, underscoring the urgent need for improved prognostic tools and treatment strategies [13, 14].

Radiomics has gained increasing attention in lung cancer research, offering deeper insights into tumor biology by enabling early detection, treatment response monitoring, and outcome prediction [15, 16]. First introduced by Dutch researcher Kumar in 2012, radiomics remains a widely debated yet promising approach in medical imaging [17]. Although there is no universally accepted definition, radiomics broadly refers to the extraction of high-dimensional, quantitative data from medical images—often capturing intricate patterns that are imperceptible to the human eye [18, 19]. By leveraging tumor segmentation, feature extraction, and model construction, radiomics provides a non-invasive means of assessing tumor heterogeneity and uncovering pathophysiological information relevant to prognosis [20]. However, owing to the relatively low incidence of SCLC among all lung cancer subtypes, studies investigating the prognostic value of radiomic features in SCLC remain limited.

A major challenge in SCLC management is predicting which patients will exhibit poor responses to initial treatment, as chemotherapy resistance inevitably develops, leading to varying relapse rates among individuals. To address this, nomograms have become widely used in oncology for cancer prognosis, offering a user-friendly tool that translates complex statistical prediction models into individualized numerical estimates [21]. These estimates, which quantify the probability of events such as survival or recurrence, help guide clinical decision-making, refine risk stratification, and facilitate personalized treatment strategies [22].

Although nomograms have been developed for predicting survival in various malignancies, limited research has explored their utility in SCLC prognosis. Therefore, this study aimed to develop and validate a clinical-radiomics nomogram incorporating clinical risk factors and a Rad-score to estimate PFS in patients with SCLC. This model has the potential to provide a more accurate and individualized prognostic assessment, ultimately aiding in clinical decision-making and improving patient outcomes.

Materials and methods

Study design and data collection

A total of 538 patients with SCLC who underwent CT examination at Huadong Hospital from January 1, 2013 to December 31, 2023 were included. Of these, 95

patients were eventually enrolled based on the inclusion and exclusion criteria. The inclusion criteria were as follows: (a) patients with histologically confirmed SCLC, (b) patients who underwent CT before treatment, and (c) patients who were followed up at least three times at our hospital. The exclusion criteria were as follows: (a) past or present history of other malignant tumors, (b) history of treatment before baseline CT scan, and (c) incomplete clinical information. The 95 patients were randomly categorized into training and validation cohorts in a 7:3 ratio. The training cohort was used to establish the nomogram. The flow chart for the study is shown in Fig. 1.

One radiologist (Y.N., two years of experience in thoracic radiology) searched picture archiving and communication systems in Huadong Hospital affiliated to Fudan University for the following clinical information: age, sex, NSE, CA199, CA125, carcinoma embryonic antigen (CEA), neutrophil-to-lymphocyte ratio (NLR), and different treatments. The primary endpoint of the investigation was PFS, which denotes the duration from the initiation of clinical treatment to either disease progression or mortality from any cause among the patients. The median follow-up period for all patients was 167.5 days, with the shortest follow-up being 90 days post-treatment and the longest extending to 970 days.

CT examination

All CT scans were performed using one of the following four scanners: GE Discovery CT750 HD (GE Healthcare, USA), 64-slice LightSpeed VCT (GE Healthcare, USA), Somatom Definition Flash (Siemens Healthcare, Germany), and Somatom Sensation-16 (Siemens Healthcare, Germany). The scan parameters were as follows: tube current was 120–200 mA; tube voltage was 80–120 kV; scan layer thickness was 1–2 mm; reconstruction algorithm was STND/medium sharp; scan phase was deep inspiratory phase; and scan body position was supine. We have indeed implemented several measures in our study to minimize potential biases arising from scanner differences, including ensuring all scanners followed a unified scanning protocol with the same imaging parameters (such as slice thickness, scanning range, etc.), as well as image preprocessing and quality control.

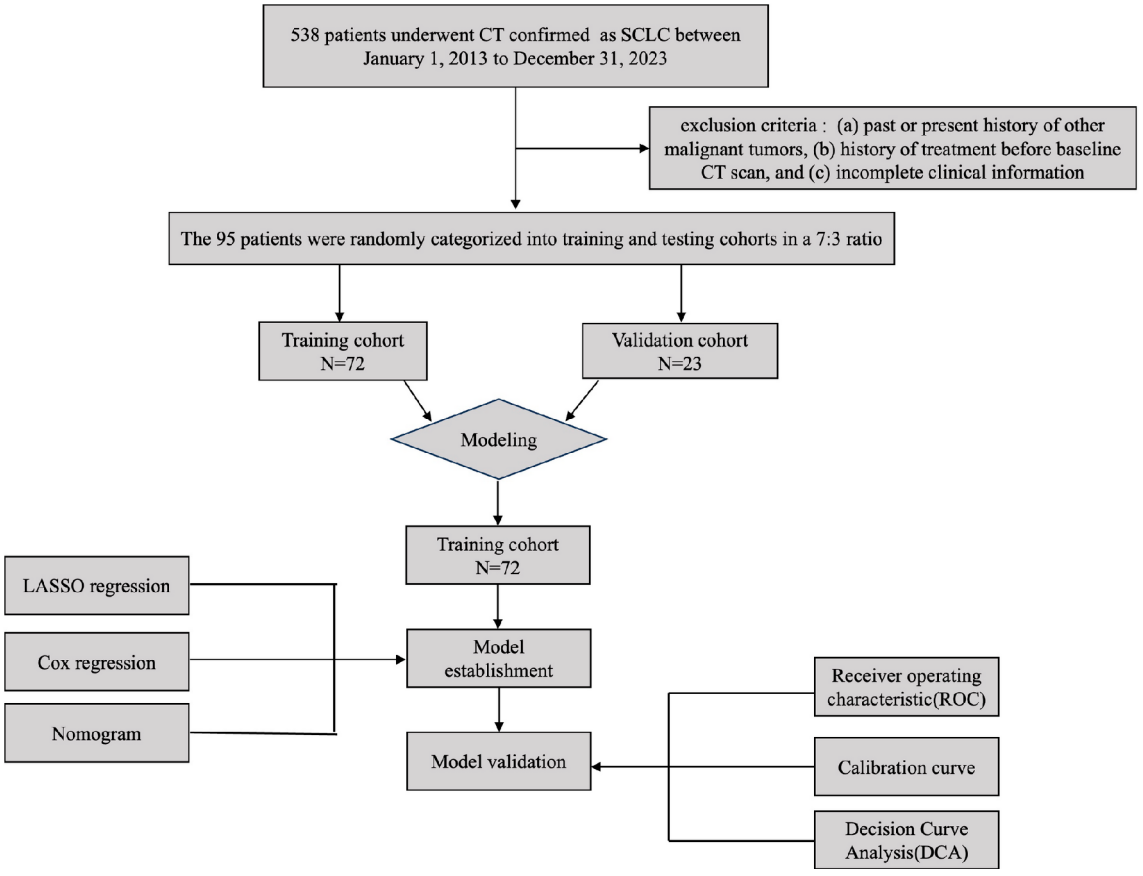

Fig. 1 Study workflow diagram. Lasso = least absolute shrinkage and selection operator, ROC = receiver operating characteristic curve, DCA = decision curve analysis

Tumor segmentation and feature extraction

Three-dimensional (3D) tumor segmentation was performed independently by two radiologists (Y.N., two years of experience in thoracic radiology; M.Z.X, six years of experience in thoracic radiology) with more than two years of experience using the 3D-SLICER software (3D Slicer, version 4.13.0; National Institutes of Health; https://www.slicer.org; accessed on August 7, 2021). Since the initial diagnosis of most patients was first performed with unenhanced CT chest examination, the unenhanced CT is more likely to provide the most original image information of the patient's lesion. Both radiologists referred to the CT enhancement examination and generated 3D tumor segmentation by manually drawing the volume of interest (VOI) along the tumor edge layer by layer until the entire tumor was covered in the unenhanced CT. To investigate the inter- and intra-observer reproducibility of the radiomics feature extraction, 30 images were randomly selected from the training set one month after the outlining was completed, and the VOI was outlined by one radiologists (Y.N.). Two-way random-effects models were used to calculate intraclass correlation coefficients (ICCs) to determine inter- and intra-observer reliability. Only the radiomics features with excellent reliability (ICC ≥ 0.75) were considered robust.

Radiomic features were extracted using Pyradiomics (version 3.0.1), and 1,218 radiomics features were extracted. The main radiomics features were first-order statistics (18 features); shape statistics (14 features); texture features including gray-level co-occurrence matrix, gray-level size zone matrix, gray-level dependence matrix, gray-level run length matrix (68 features); statistical features derived from texture matrices in Laplacian of Gaussian filtered domain (1.0–5.0 mm kernels; 430 features); and statistical features derived from texture matrices in wavelet filtered domains (688 features).

Feature selection and Rad-score calculation

The performance of a predictive model depends on the amount of useful information. Therefore, to enhance model stability and prevent overfitting, it is crucial to remove irrelevant features. Radiomics features from the training cohort were evaluated using LASSO, univariate and multivariate Cox analyses to determine the association between each feature and PFS, and features with $p < 0.05$ were used for rad-score calculation. Five radiomics features were ultimately selected for rad-score calculation. The rad-score was calculated for each patient by weighting the respective coefficients using a linear combination of the selected features. The radiomics flow chart of the study is shown in Fig. 2.

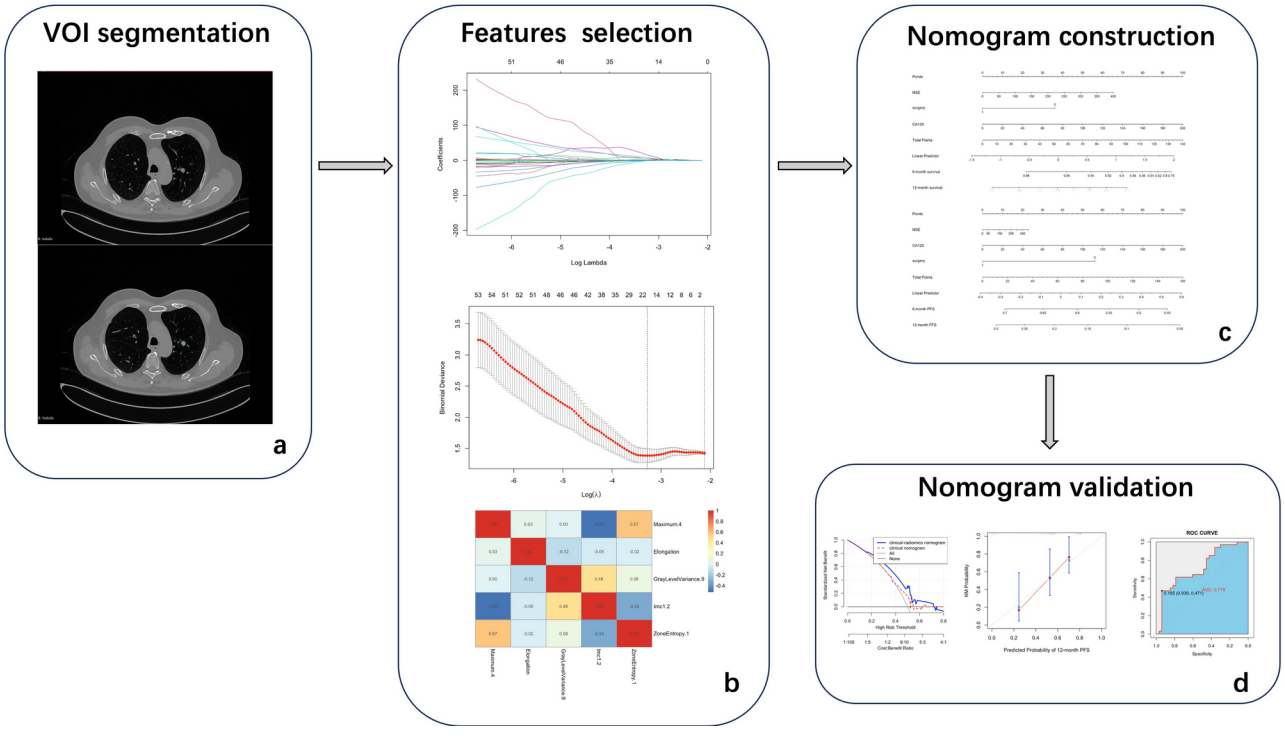

Fig. 2 The radiomics flow chart of the study. (**a**) VOI segmentation (**b**) Features selection including lasso Coefficient path diagram, lasso Regression analysis cross plot, the correlation heatmap (**c**) nomogram construction including clinical nomogram and clinical-radiomics nomogram (**d**) nomogram validation including DCA, calibration curve and ROC

Construction and validation of the nomogram

For the 12 clinical risk factors, including age, sex, different treatment modalities (chemotherapy, radiotherapy, immunotherapy, and surgery), tumor markers (CEA, CA199, CA125, cytokeratin 19 fragment, and NSE), and NLR, univariate and multivariate Cox analyses were performed to test the correlation between each risk factor and the patient's PFS, and $p < 0.05$ in the univariate Cox analyses were included in the development of the clinical nomogram (Fig. 3a).

A total of 21 statistical features were selected using LASSO. Then, univariate and multivariate Cox analyses ($p < 0.05$) were carried out to identify the optimized subset of radiomics features. Eventually, five radiomics features were selected for rad-score calculation, and a clinical-radiomics nomogram was developed (Fig. 3b).

In the training cohort, patients were classified into low- and high-risk groups based on the rad-score, and their optimal cut-off values were determined and analyzed using Kaplan-Meier survival analysis with the cut-off package in R Studio (Fig. 4a). Each model's performance in predicting PFS was analyzed based on the area under the curve (AUC) values for the receiver operating characteristic (ROC) curves in the training and validation cohorts. ROC curves were plotted for the training and validation cohorts for 6- and 12-month PFS (Fig. 5). The performance of the clinical and radiomics-clinical nomograms were analyzed using calibration curves and decision curve analysis (Figs. 4b and 6). Calibration curves of the nomogram were used to evaluate the consistency between actual and predicted survival outcomes. This

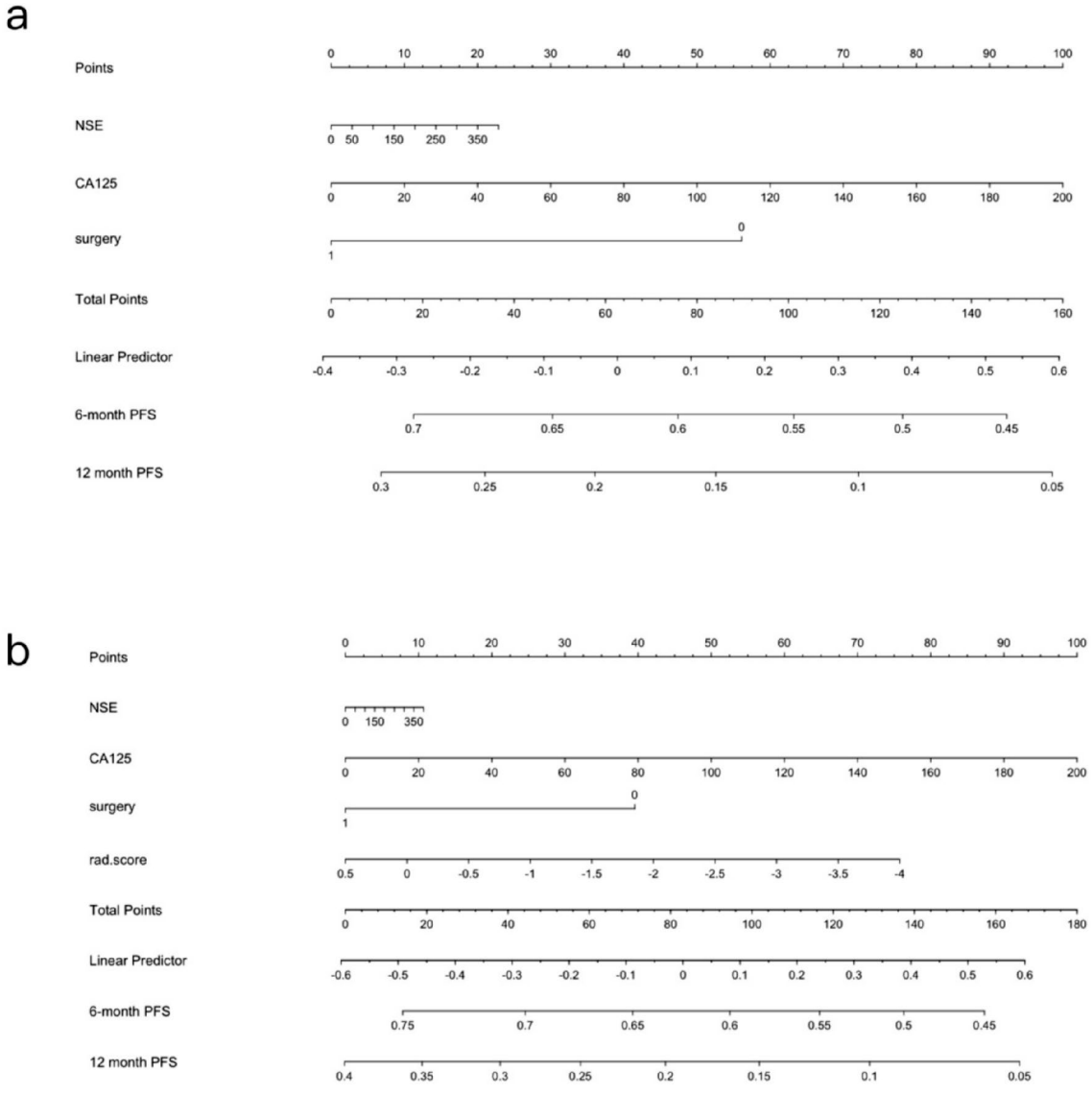

Fig. 3 (**a**) clinical nomogram (**b**) clinical-radiomics fusion nomogram

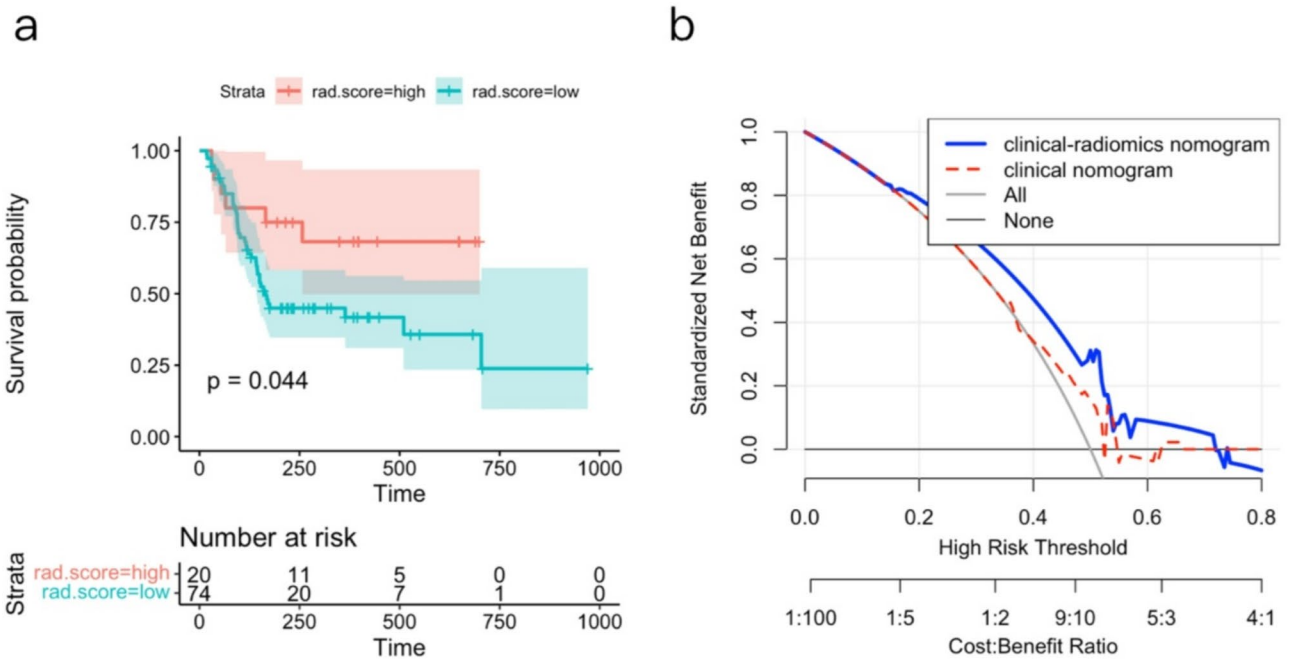

Fig. 4 (**a**) Kaplan-Meier progression-free survival (PFS) curves of patients at different risks stratified by the Rad-score in the training cohort. (**b**) decision curve analysis for each nomogram in the training cohort. The y-axis measures the net benefit. The clinical-radiomics nomogram (solid blue line) had a higher net benefit compared with the clinical nomogram (red dotted line)

approach allows for a comparative assessment of PFS and the accuracy of the developed nomograms.

Statistical analysis

All statistical analyses were performed using R studio software, version 4.1.0 (https://www.r-project.org/) and a commercially available software program SPSS 23.0 for Windows (SPSS, Chicago, IL, USA). The packages in R studio software used in the current study included "rms," "survival," "Hmisc," "timeROC," "ggplot2," and "survminer." Continuous variables were expressed as means ± standard deviations and compared using the independent samples t-test or Kruskal–Wallis test. Categorical variables were expressed as frequencies and analyzed using the chi-square or Fisher's exact test. The AUC for the ROC curve was used to evaluate the predictive effectiveness of the model. Calibration curves were plotted to assess the accuracy of the nomogram predictions. Clinical decision curves were utilized to evaluate the clinical usefulness of the models. Statistical significance was set at a two-sided p-value of < 0.05.

Before analysis, we assessed the missing data. Missing data were handled using deletion and imputation methods. For variables with a low missing rate, median imputation was applied for continuous variables, while mode imputation was used for categorical variables. For variables with a high missing rate, considering the potential bias introduced by excessive missing values, they were excluded from the final analysis.

Result

The clinical characteristics of the 95 enrolled patients are shown in Table 1. The median age was 68 years (range: 46–83); 11 patients were women (12%) and 84 were men (88%). There were no statistically significant differences in the distribution of clinical features between the training and validation cohorts.

Initially, participants were randomly categorized into training and validation cohorts. In the training cohort, univariate and multivariate analyses using Cox regression were conducted to identify the significant clinical risk factors influencing PFS. Subsequently, factors with a significance level of $p < 0.05$ in the univariate Cox analysis were selected to formulate the clinical nomogram, enabling the prediction of 6-month and 12-month PFS in patients with SCLC. Univariate Cox regression analysis revealed that surgery, NSE, and CA125 levels were significantly associated with PFS in the training cohort (all $p < 0.05$; Table 2). These features were used to develop a nomogram.

Thirty patients were randomly selected from the training cohort and delineated again by Y. N. one month after the initial analysis. The results of the inter- and intra-observer Bland-Altman plots showed a high level of agreement between observers Y. N. The intra-observer consistency was higher than the inter-observer consistency.

Twenty-one radiomics features with statistically significant differences were selected using LASSO. Univariate

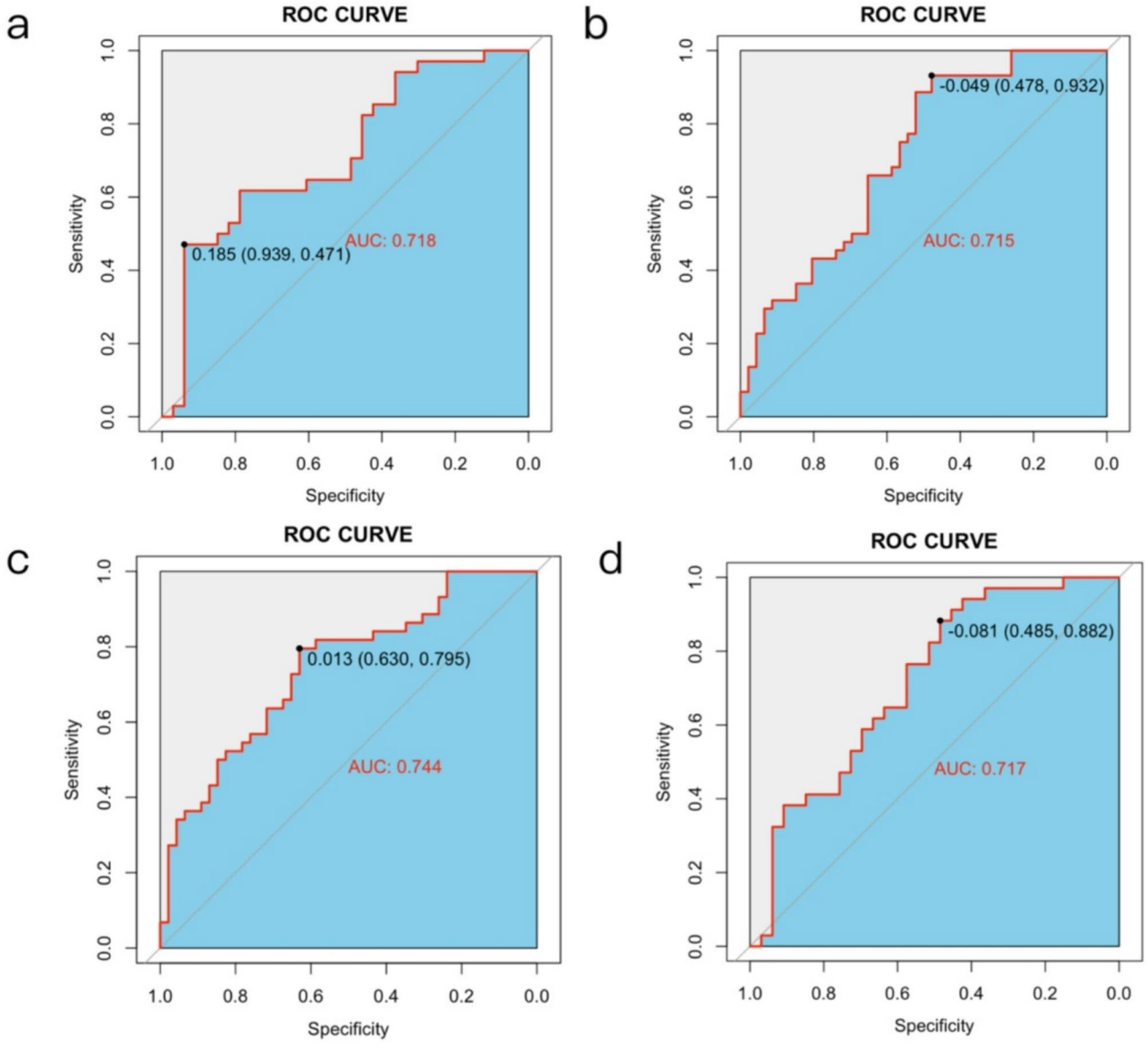

Fig. 5 The ROC curves for the training and validation cohorts. (**a**) training cohort for clinical nomogram. (**b**)validation cohort for clinical nomogram. (**c**) training cohort for clinical-radiomics nomogram. (**d**) validation cohort for clinical-radiomics nomogram

and multivariate Cox analyses ($p < 0.05$) was carried out to select the optimized subset of radiomics features to construct the final model. The rad-score was calculated by summing the selected radiomics features weighted by their coefficients and constructing a clinical-radiomics nomogram. The most predictive subset of features was selected after determining the number of features, and their corresponding coefficients were evaluated.

A nomogram containing variables independent of clinical risk factors and the rad-score was associated with PFS. A PFS of 6-month or 12-month can be calculated by summing the points corresponding to the patients' characteristics. The images are shown in Fig. 3.

Validation of the nomogram

The ROC curve was used to evaluate the model's performance. Radiomic signatures in the training cohort were significantly associated with PFS (hazard ratio: 0.5765, 95% confidence interval (CI): 0.3641–0.9128, $p < 0.05$). The clinical nomogram model and clinical-radiomics nomogram model in the training cohort achieved AUCs of 0.718 (95% CI: 0.471,0.939), and 0.744 (95% CI: 0.630, 0.795), respectively. The clinical nomogram and clinical-radiomics nomogram models in the validation cohort achieved AUCs of 0.715 (95% CI: 0.478, 0.932) and 0.717 (95% CI: 0.485, 0.882), respectively. In both the training and validation cohorts, the clinical-radiomics nomogram model performed significantly better than the clinical

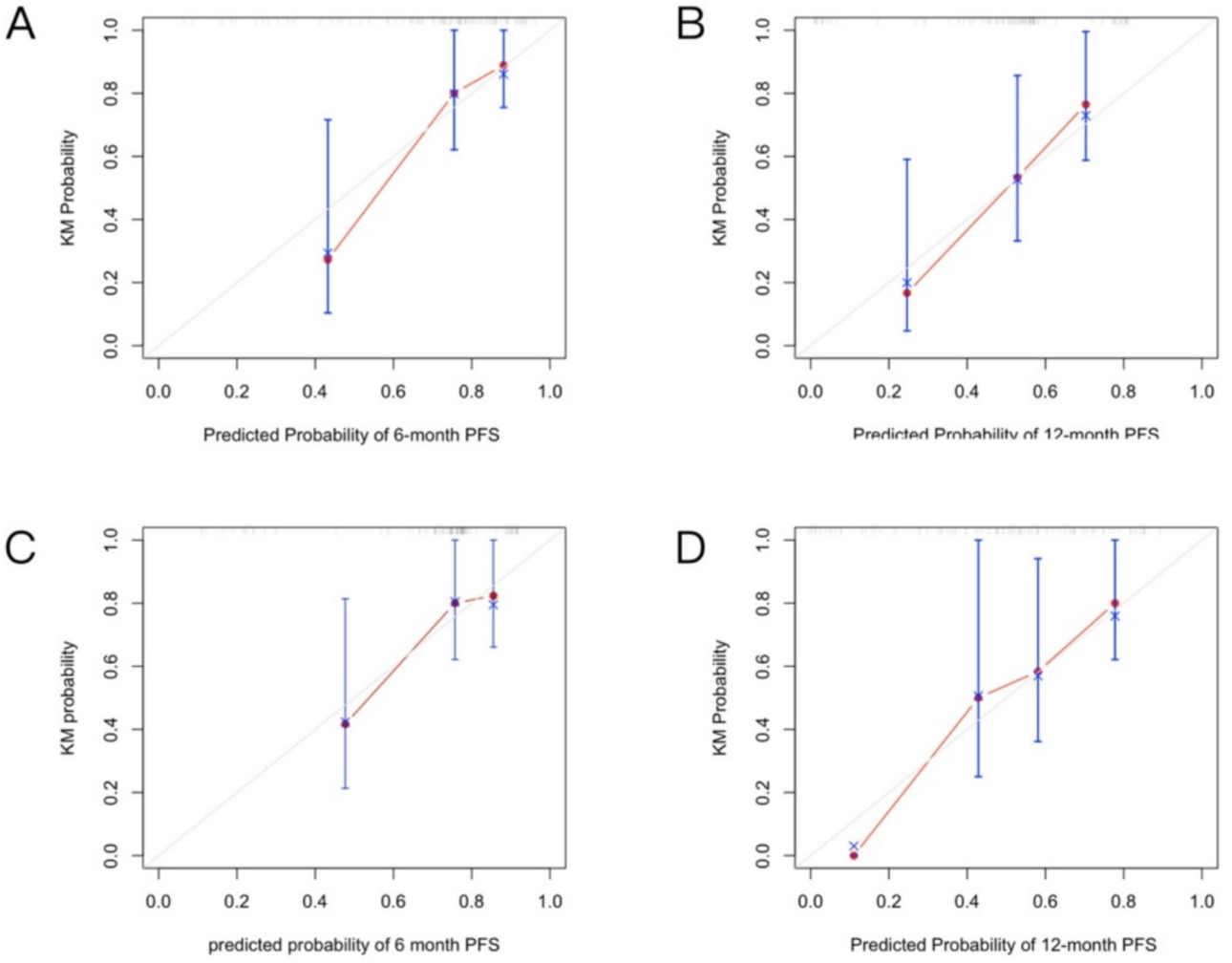

Fig. 6 Plot shows a calibration of the clinical nomogram and clinical-radiomics nomogram in terms of agreement between predicted and observed 6-, and 12-months PFS outcomes in the training cohort. (**a**) 6-month calibration curves for clinical nomogram. (**b**) 12-month calibration curves for clinical nomogram. (**c**) 6-month calibration curves for clinical-radiomics nomogram. (**d**) 12-month calibration curves for clinical-radiomics nomogram

nomogram models. These findings reflect the good diagnostic performance of radiomics features in both the training and validation cohorts.

Calibration and clinical utility of models

The calibration curve for the nomogram showed good calibration in both training and validation cohorts(Fig. 6). The decision curve suggested that in both the training and validation cohorts, the clinical-radiomics nomogram performed slightly better than the clinical nomogram(Fig. 4b).

Discussion

This study established a nomogram model that combines clinical risk factors, and radiomics features to predict PFS in patients with SCLC. It showed the best performance in the training and validation cohort. The clinical-radiomics model outperformed the clinical model in the training and validation cohort, and the addition of rad-score information significantly improved the model's performance. This model can help formulate a scientific and standardized follow-up strategy and improve the effectiveness of diagnosis and treatment.

This study established and validated a nomogram based on 95 patients from Huadong Hospital affiliated with Fudan University. The nomogram was used to predict the 6-month and 12-month PFS of patients with SCLC according to three clinical factors—NSE, surgery, and CA125 — along with the rad-score. More importantly, the radiomics-clinical nomogram developed in this study had reliable predictive performance, was significantly superior to clinical risk factors, and provided effective support for the implementation of individualized SCLC information.

Nomograms can be used for the prognostic assessment of various tumors [23, 24]. Radiomics is widely used in

Table 1 Clinical characteristics of patient with SCLC in the training and validation cohorts

Variables	Training cohort($n=72$)	validation cohort($n=23$)	*P* value
Age(years), $\mu \pm \sigma$	67.31 ± 8.136	64.8 ± 6.648	0.358
Sex (%)			0.531
Female	7(9.7)	4(17.4)	
Male	65(90.3)	19(82.6)	
Chemotherapy (%)			0.579
Yes	64(88.9)	22(95.7)	
No	8(11.1)	1(4.3)	
Radiotherapy (%)			0.311
Yes	11(15.3)	1(4.3)	
No	61(84.7)	22(95.7)	
Surgery (%)			0.209
Yes	17(23.6)	2(8.7)	
No	55(76.7)	21(9.3)	
Immunotherapy (%)			0.841
Yes	16(22.2)	4(17.4)	
No	56(77.8)	19(82.6)	
CEA (ng/ml), median(IQR)	3.950(2.625,5.950)	11.400(7.900,19.900)	0.990
NSE (ng/ml), median(IQR)	24.600(13.875,41.600)	73.700(21.300,122.900)	0.001
NLR, median	2.540(2.103,3.609)	3.165(2.416,3.728)	0.068
CYFRA 21 – 1 (ng/ml), median (IQR)	3.270(2.560,4.180)	4.070(2.950,6.200)	0.049
CA125(ng/ml), median(IQR)	15.600(9.750,25.775)	27.100(13.800,41.700)	0.026
CA199(ng/ml), median(IQR)	10.700(7.300,22.800)	11.400(7.900,19.900)	0.925

CEA: Carcinoma embryonic antigen NSE: Neuron specific enolase CYFRA 21 – 1: Cytokeratin fragment 19 CA199: Carbohydrate antigen 199 CA125: Carbohydrate antigen 125 IQR: Interquartile range

clinical research to extract subtle but clinically relevant information from imaging data, which can reflect spatial heterogeneity, tumor microenvironment, and gene expression [25]. However, most studies have focused on non-SCLC, which has a high incidence and requires more sophisticated treatment programs, while limited research has been done on SCLC [26, 27]. Currently, few studies have been conducted on the use of nomograms to predict SCLC prognosis. Yaji Yang et al. [28] used age, histologic typing, tumor size, and stage to establish a nomogram for predicting 1-, 3-, and 5-year survival rates. Unlike our study, their study only included clinical information about the patients and lesion characteristics. It did not include the radiomics features of the lesions and different treatments, thus limiting the application of the model. Wang et al. [29] used age, race, sex, staging, and treatment modalities to incorporate nomogram development into a survival analysis. However, the clinical variables they adopted did not incorporate current emerging therapies such as immunotherapy, and various tumor markers. Our advantage lies in the complete application of clinical variables and radiomics features. It is important to assess PFS in patients with SCLC, and we found that radiomics features were significantly associated with PFS.

The treatment of SCLC has been stagnant for many years; in recent years, new opportunities have arisen owing to the initial experience with immunotherapeutic agents. Chemotherapy with etoposide in combination with platinum is the first-line treatment for SCLC [12]. However, some studies have shown that immunotherapy combined with chemotherapy can prolong patient survival, including overall survival (OS) and PFS. For instance, the IMpower133 [10] enrolled patients treated with chemotherapy in combination with either Atezolizumab or a placebo, median OS was significantly prolonged by 2.0 months in the Atezolizumab combination group compared with the control group (12.3 vs. 10.3 months, $P=0.0154$), with median PFS of 5.2 vs. 4.3 months, respectively.

While surgery is a risk-opportunity treatment, it is often used in patients diagnosed at an early stage. Some patients experience serious postoperative complications or even death [30]. Early stage LS-SCLC with lesions limited to a single lobe and in good condition is more suitable for surgical resection, and the 5-year survival rate of early-stage patients with lobectomy can reach 30 ~ 58%, which confirms the irreplaceable status of surgery in the treatment of early-stage LS-SCLC [31, 32].

The radiomics-based nomogram developed in this study extracts a large number of high-dimensional, quantitative features from CT, integrating information on tumor heterogeneity, morphology, and texture. This enables personalized recurrence risk assessment and the formulation of tailored follow-up and treatment plans for patients. The model holds significant clinical value in prognostic prediction for SCLC patients.

First, the nomogram provides quantitative and intuitive risk scores, allowing clinicians to quickly interpret and apply the results. By setting specific risk thresholds, clinicians can determine whether a patient requires more intensive follow-up or proactive therapeutic interventions. Second, this model significantly improves the accuracy and reliability of recurrence risk assessment compared to traditional clinical and imaging indicators. By incorporating radiomic features, it captures micro-level tumor biology that conventional prognostic tools may overlook, enabling a more refined risk stratification. Moreover, the nomogram highlights the contribution

Table 2 Univariate and multivariable Cox regression analyses in training cohort comprising 95 patients with small cell lung cancer

	Univariate cox regression		Multivariable cox regression			
	HR(95%CI)	*P* value	Clinical model		Clinical-radiomics model	
			HR(95%CI)	*P* value	HR(95%CI)	*P* value
Age	1.000(0.956–1.046)	0.986	NA	NA	NA	NA
Sex	0.572(0.172–1.906)	0.363	NA	NA	NA	NA
Chemotherapy	0.240(0.053–1.096)	0.117	NA	NA	NA	NA
Radiotherapy	0.868(0.413–1.826)	0.710	NA	NA	NA	NA
Immunotherapy	1.353(0.676–2.710)	0.394	NA	NA	NA	NA
Surgery	0.338(0.159–0.717)	0.005	0.408(0.187–0.889)	0.0242	0.520(0.230–1.177)	0.1168
CEA	0.985(0.961–1.009)	0.208	NA	NA	NA	NA
NSE	1.005(1.002–1.009)	0.003	1.004(1.000-1.008)	0.051	1.003(0.000-1.008)	0.132
NLR	1.110(0.780–1.580)	0.561	NA	NA	NA	NA
CA199	1.008(0.996–1.019)	0.208	NA	NA	NA	NA
CA125	1.016(1.005–1.026)	0.004	1.012(1.000-1.024)	0.039	1.014(1.001–1.026)	0.028
CYFRA 21 – 1	0.977(0.879–1.085)	0.662	NA	NA	NA	NA
Radiomics signature	0.605(0.407–0.899)	$P < 0.001$	NA	NA	0.577(0.364–0.913)	0.019

HR: Hazard ratio CI: Confidence interval CEA: Carcinoma embryonic antigen NSE: Neuron specific enolase CYFRA 21 – 1: Cytokeratin fragment 19 CA199: Carbohydrate antigen 199 CA125: Carbohydrate antigen NLR: Neutrophil-to-lymphocyte ratio

of different features to recurrence time through their respective weights, offering valuable insights for future research on the biological mechanisms of SCLC.

Compared to previous studies, this research offers significant advantages in predicting PFS in SCLC. First, it innovatively integrates radiomic features with clinical risk factors, overcoming the limitations of models based solely on clinical characteristics or radiomics, resulting in a more comprehensive and accurate predictive model. Unlike traditional clinical staging systems, the nomogram developed in this study extracts a large number of high-dimensional, quantitative features from non-invasive CT, providing in-depth insights into tumor morphology, texture, and heterogeneity for personalized recurrence risk assessment. In terms of clinical applicability, this study employs a nomogram as an intuitive tool, allowing physicians to quickly interpret and apply predictive results. Additionally, the nomogram's feature weighting analysis highlights the contribution of different radiomic features to recurrence timing, providing crucial insights into the biological mechanisms of SCLC.

However, this study had certian limitations. Although the nomogram offers a certain level of interpretability in prediction, its direct application to clinical decision-making has notable limitations. Firstly, the accuracy of the radiomics model is highly dependent on the quality and consistency of the imaging data. Inadequate feature selection can lead to issues such as model overfitting, while a small sample size can undermine the model's generalizability. In future studies, we plan to use external validation sets to further validate the model, ensuring its robustness and effectiveness in clinical practice. In addition, both the retrospective study design and the manual lesion mapping were subject to bias. In future research, we will adopt more innovative technologies to further enhance the model's performance. This includes exploring the integration of deep learning with traditional radiomics feature extraction, multimodal data, and optimization algorithms. These approaches aim to more comprehensively characterize tumor heterogeneity and improve the accuracy and robustness of the model's predictions. To enhance the model's robustness and generalizability, we plan to collect large-scale, heterogeneous datasets from multiple centers to validate the model's performance and explore its applicability across different patient populations.

Conclusions

In conclusion, we established a model to predict the probability of PFS by combining clinical and radiomics information, which is better than the clinical model and can predict the probability of PFS more accurately. This model can provide more information about SCLC and individualized treatment strategies.

Abbreviations

SCLC	Small cell lung cancer
ES-SCLC	Extensive stage small cell lung cancer
PFS	Progression-free survival
CT	Computed tomography
DCA	Decision curve Analysis
ICC	Intraclass correlation coefficient
LASSO	Least absolute shrinkage and selection operator
CA199	Carbohydrate antigen 199
CA125	Carbohydrate antigen 125
ROC	Receiver operating characteristic curve
AUC	Area under the curve
VOI	Region of interest
CEA	Carcinoma embryonic antigen
NLR	Neutrophil-to-lymphocyte ratio
NSE	Neuron specific enolase
OS	Overall survival
CI	Confidence interval
C-index	Concordance index
rad-score	Radiomics score

Author contributions
Ming Li and Liang Jin is the guarantor of integrity for the entire study and supervised the study. Nan Yang designed the study, reviewed the literature, conducted clinical data and statistical analyses, and drafted and revised the manuscript. Zhuangxuan Ma, Xin Wang and Li Xiao conducted clinical data and statistical analyses and drafted and revised the manuscript. All authors reviewed the manuscript, contributed to the article, and approved the submitted version.

Funding
This study was supported by the National Key Research and Development Program 2022YFF1203301 (Ming Li), National Natural Science Foundation of China 61976238 (Ming Li), Science and Technology Planning Project of Shanghai Science and Technology Commission 22Y11910700 (Liang Jin), Science and Technology Planning Project of Shanghai Science and Technology Commission 20Y11902900 (Ming Li), Shanghai "Rising Stars of Medical Talent" Youth Development Program "Outstanding Youth Medical Talents" SHWJRS [2021]-99 (Ming Li), Cancer Society of Shanghai SACA-CY21C12 (Yingli Sun), Emerging Talent Program (XXRC2213), and Leading Talent Program (LJRC2202).

Data availability
The raw datasets supporting the conclusions of this article are available from the corresponding author on reasonable request.

Declarations

Ethics approval and consent to participate
This study was approved by the Institutional Ethics Committee of Huadong Hospital, Affiliated with Fudan University, which waived the requirement for informed consent. All procedures were carried out in accordance with the relevant guidelines and regulations, and the study was conducted in accordance with the principles of the Declaration of Helsinki.

Consent for publication
Not applicable.

Competing interests
The authors declare no competing interests.

Author details
[1]Department of Radiology, Huadong Hospital, Fudan University, Shanghai 200040, China
[2]Department of Pathology, Huadong Hospital, Fudan University, Shanghai 200040, China
[3]Zhang Guozhen Small Pulmonary Nodules Diagnosis and Treatment Center, Shanghai 200040, China

Received: 18 October 2024 / Accepted: 25 April 2025
Published online: 06 May 2025

References

1. Wang Q, Gumus ZH, Colarossi C, Memeo L, Wang X, Kong CY, Boffetta P. SCLC: epidemiology, risk factors, genetic susceptibility, molecular pathology, screening, and early detection. J Thorac Oncol. 2023;18(1):31–46. https://doi.org/10.1016/j.jtho.2022.10.002.
2. Siegel RL, Miller KD, Wagle NS, Jemal A. Cancer statistics, 2023. CA Cancer J Clin. 2023;73(1):17–48. https://doi.org/10.3322/caac.21763.
3. Bernhardt EB, Jalal SI. Small cell lung Cancer. Cancer Treat Res. 2016;170:301–22. https://doi.org/10.1007/978-3-319-40389-2_14.
4. Gazdar AF, Bunn PA, Minna JD. Small-cell lung cancer: what we know, what we need to know and the path forward. Nat Rev Cancer. 2017;17(12):725–37. https://doi.org/10.1038/nrc.2017.87.
5. Yang S, Zhang Z, Wang Q. Emerging therapies for small cell lung cancer. J Hematol Oncol. 2019;12(1):47. https://doi.org/10.1186/s13045-019-0736-3.
6. Silva M, Galeone C, Sverzellati N, Marchianò A, Calareso G, Sestini S, La Vecchia C, Sozzi G, Pelosi G, Pastorino U. Screening with Low-Dose computed tomography does not improve survival of small cell lung Cancer. J Thorac Oncol. 2016;11(2):187–93. https://doi.org/10.1016/j.jtho.2015.10.014.
7. Bogart JA, Waqar SN, Mix MD. Radiation and systemic therapy for Limited-Stage Small-Cell lung Cancer. J Clin Oncol. 2022;40(6):661–70. https://doi.org/10.1200/JCO.21.01639.
8. Chung T-W, Su J-H, Lin C-C, Li Y-R, Chao Y-H, Lin S-H, Chan H-L. 24-Methyl-Cholesta-5, 24(28)-Diene-3β, 19-diol-7β-Monoacetate inhibits human small cell lung Cancer growth in vitro and in vivo via apoptosis induction. Mar Drugs. 2017;15(7). https://doi.org/10.3390/md15070210.
9. Remon J, Aldea M, Besse B, Planchard D, Reck M, Giaccone G, Soria JC. Small cell lung cancer: a slightly less orphan disease after immunotherapy. Ann Oncol. 2021;32(6):698–709. https://doi.org/10.1016/j.annonc.2021.02.025.
10. Liu SV, Reck M, Mansfield AS, Mok T, Scherpereel A, Reinmuth N, Garassino MC, De Castro Carpeno J, Califano R, Nishio M, et al. Updated overall survival and PD-L1 subgroup analysis of patients with Extensive-Stage Small-Cell lung Cancer treated with Atezolizumab, carboplatin, and Etoposide (IMpower133). J Clin Oncol. 2021;39(6):619–30. https://doi.org/10.1200/JCO.20.01055.
11. Dingemans AMC, Früh M, Ardizzoni A, Besse B, Faivre-Finn C, Hendriks LE, Lantuejoul S, Peters S, Reguart N, Rudin CM, et al. Small-cell lung cancer: ESMO clinical practice guidelines for diagnosis, treatment and follow-up☆. Ann Oncol. 2021;32(7):839–53. https://doi.org/10.1016/j.annonc.2021.03.207.
12. Paz-Ares L, Dvorkin M, Chen Y, Reinmuth N, Hotta K, Trukhin D, Statsenko G, Hochmair MJ, Özgüroğlu M, Ji JH, et al. Durvalumab plus platinum-etoposide versus platinum-etoposide in first-line treatment of extensive-stage small-cell lung cancer (CASPIAN): a randomised, controlled, open-label, phase 3 trial. Lancet. 2019;394(10212):1929–39. https://doi.org/10.1016/S0140-6736(19)32222-6.
13. Sung H, Ferlay J, Siegel RL, Laversanne M, Soerjomataram I, Jemal A, Bray F. Global Cancer statistics 2020: GLOBOCAN estimates of incidence and mortality worldwide for 36 cancers in 185 countries. CA Cancer J Clin. 2021;71(3):209–49. https://doi.org/10.3322/caac.21660.
14. Franco F, Carcereny E, Guirado M, Ortega AL, López-Castro R, Rodríguez-Abreu D, García-Campelo R, Del Barco E, Juan O, Aparisi F, et al. Epidemiology, treatment, and survival in small cell lung cancer in Spain: data from the thoracic tumor registry. PLoS ONE. 2021;16(6):e0251761. https://doi.org/10.1371/journal.pone.0251761.
15. Guo Y, Song Q, Jiang M, Guo Y, Xu P, Zhang Y, Fu C-C, Fang Q, Zeng M, Yao X. Histological subtypes classification of lung cancers on CT images using 3D deep learning and radiomics. Acad Radiol. 2021;28(9):e258–66. https://doi.org/10.1016/j.acra.2020.06.010.
16. Thawani R, McLane M, Beig N, Ghose S, Prasanna P, Velcheti V, Madabhushi A. Radiomics and radiogenomics in lung cancer: A review for the clinician. Lung Cancer. 2018;115:34–41. https://doi.org/10.1016/j.lungcan.2017.10.015.
17. Kumar V, Gu Y, Basu S, Berglund A, Eschrich SA, Schabath MB, Forster K, Aerts HJWL, Dekker A, Fenstermacher D, et al. Radiomics: the process and the challenges. Magn Reson Imaging. 2012;30(9):1234–48. https://doi.org/10.1016/j.mri.2012.06.010.
18. Gillies RJ, Kinahan PE, Hricak H. Radiomics: images are more than pictures, they are data. Radiology. 2016;278(2):563–77. https://doi.org/10.1148/radiol.2015151169.
19. Yip SSF, Aerts HJWL. Applications and limitations of radiomics. Phys Med Biol. 2016;61(13):R150. https://doi.org/10.1088/0031-9155/61/13/R150.
20. Liu Z, Wang S, Dong D, Wei J, Fang C, Zhou X, Sun K, Li L, Li B, Wang M, et al. The applications of radiomics in precision diagnosis and treatment of oncology: opportunities and challenges. Theranostics. 2019;9(5):1303–22. https://doi.org/10.7150/thno.30309.
21. Balachandran VP, Gonen M, Smith JJ, DeMatteo RP. Nomograms in oncology: more than Meets the eye. Lancet Oncol. 2015;16(4):E173–80. https://doi.org/10.1016/s1470-2045(14)71116-7.
22. Iasonos A, Schrag D, Raj GV, Panageas KS. How to build and interpret a nomogram for cancer prognosis. J Clin Oncol. 2008;26(8):1364–70. https://doi.org/10.1200/jco.2007.12.9791.
23. Wang RJ, Dai WX, Gong J, Huang MZ, Hu TD, Li H, Lin KL, Tan C, Hu H, Tong T, et al. Development of a novel combined nomogram model integrating deep learning-pathomics, radiomics and immunoscore to predict postoperative outcome of colorectal cancer lung metastasis patients. J Hematol Oncol. 2022;15(1). https://doi.org/10.1186/s13045-022-01225-3.
24. Guo QK, Yang HS, Shan SC, Chang DD, Qiu LJ, Luo HH, Li HP, Ke ZF, Zhu Y. A radiomics nomogram prediction for survival of patients with driver gene-negative lung adenocarcinomas (LUAD). Radiologia Med. 2023;128(6):714–25. https://doi.org/10.1007/s11547-023-01643-4.
25. Gatenby RA, Grove O, Gillies RJ. Quantitative imaging in cancer evolution and ecology. Radiology. 2013;269(1). https://doi.org/10.1148/radiol.13122697.

26. Liu C, Zhao W, Xie J, Lin H, Hu X, Li C, Shang Y, Wang Y, Jiang Y, Ding M, et al. Development and validation of a radiomics-based nomogram for predicting a major pathological response to neoadjuvant immunochemotherapy for patients with potentially resectable non-small cell lung cancer. Front Immunol. 2023;14. https://doi.org/10.3389/fimmu.2023.1115291.
27. Tong C, Miao Q, Zheng J, Wu J. A novel nomogram for predicting the decision to delayed extubation after thoracoscopic lung cancer surgery. Ann Med. 2023;55(1):800–7. https://doi.org/10.1080/07853890.2022.2160490.
28. Yang Y, Sun S, Wang Y, Xiong F, Xiao Y, Huang J. Development and validation of nomogram for predicting survival of elderly patients with stage I small-cell lung cancer. Bosnian J Basic Med Sci. 2021;21(5):632–41. https://doi.org/10.17305/bjbms.2020.5420.
29. Wang S, Yang L, Ci B, Maclean M, Gerber DE, Xiao G, Xie Y. Development and validation of a nomogram prognostic model for SCLC patients. J Thorac Oncol. 2018;13(9):1338–48. https://doi.org/10.1016/j.jtho.2018.05.037.
30. Nathan H, Yin HY, Wong SL. Postoperative complications and Long-Term survival after complex Cancer resection. Ann Surg Oncol. 2017;24(3):638–44. https://doi.org/10.1245/s10434-016-5569-5.
31. Hou SZ, Cheng ZM, Wu YB, Sun Y, Liu B, Yuan MX, Wang XD. Evaluation of short-term and long-term efficacy of surgical and non-surgical treatment in patients with early-stage small cell lung cancer: A comparative study. Cancer Biomarkers. 2017;19(3):249–56. https://doi.org/10.3233/cbm-160332.
32. Al Zreibi C, Gibault L, Fabre E, Le Pimpec-Barthes F. [Surgery for small-cell lung cancer]. Rev Mal Respir. 2021;38(8):840–7. https://doi.org/10.1016/j.rmr.2021.05.008.

Publisher's note